

Measurement and analysis techniques for a study of $^{12}\text{C}(p, \gamma)$ and $^{13}\text{C}(p, \gamma)$ deep underground

Jakub Skowronski* for the LUNA collaboration

¹Università degli Studi di Padova and INFN, Sezione di Padova, Via Francesco Marzolo 8, 35131 Padova, Italy

Abstract. The $^{12}\text{C}(p, \gamma)$ and $^{13}\text{C}(p, \gamma)$ reaction cross sections are currently under investigation in the low-background environment of the Laboratory for Underground Nuclear Astrophysics. Both reactions are being studied using different types of solid targets, and employing complementary detection techniques (HPGe spectroscopy, total absorption spectroscopy and activation counting). To reduce systematic uncertainties, targets must be accurately characterized and their degradation monitored under the intense ($\sim 400 \mu\text{A}$) beam of the LUNA-400 accelerator. We present the experimental techniques employed, and the analyses developed for the study of these reactions.

1 Introduction

The reactions $^{12}\text{C}(p, \gamma)^{13}\text{N}$ and $^{13}\text{C}(p, \gamma)^{14}\text{N}$ are the first two of the CNO cycle, which is active in the hydrogen burning regions of main sequence, Red Giant Branch (RGB) and Asymptotic Giant Branch stars (AGB). This not only contributes to the energy production, by converting four protons into one helium nucleus, but also governs the abundances of several elements. The ^{13}C is produced by the $^{12}\text{C}(p, \gamma)^{13}\text{N}$ and the subsequent β^+ decay to ^{13}C . Then it is depleted by the $^{13}\text{C}(p, \gamma)^{14}\text{N}$. Hence, both of the reactions play a key role in governing the $^{12}\text{C}/^{13}\text{C}$ ratio.

Presently the $^{12}\text{C}/^{13}\text{C}$ ratio in the Solar System is estimated to be of about 90 ± 10 [1]. One of the possible origins for the elements in the Solar System are the AGB stars [2], which are remarkably prolific centers of nucleosynthesis. Unfortunately the AGB phase of stellar evolution is marked by intense mixing phenomena, which make the theoretical models particularly difficult to establish [3]. The mixing heavily impacts the atmospheric abundance of both the ^{12}C and ^{13}C , and can arise from several different sources: convective motion inside the star, the angular momentum of the star [4], magnetic buoyancy [5] or gravitational waves [6].

Since the predictions depend on nuclear reaction rates, it is of particular interest to constrain the latter as much as possible. This can help to study the mixing phenomena in more detail and thus to constrain theoretical models. The ^{12}C and ^{13}C are the perfect candidates for this: not only are they the isotopes that burn at lowest energies, but also their ratio can be readily derived from stellar spectra.

A direct measurement of the $^{12}\text{C}(p, \gamma)^{13}\text{N}$ and $^{13}\text{C}(p, \gamma)^{14}\text{N}$ cross-sections at astrophysical energies was the goal of a recently conducted experiment at LUNA.

*e-mail: jakub.skowronski@pd.infn.it

2 Current Status

The $^{12}\text{C}(p,\gamma)^{13}\text{N}$ reaction has been studied by several experiments in the past. The S -factors reported in literature are shown in Fig. 1. Down to 200 keV there are two main data sets [7, 8], which are mostly in agreement and have been confirmed by a later measurement [9]. However, the S -factor is not properly constrained by the data reported below 200 keV. Results by [10] and [11] poorly overlap and are affected by high uncertainties, up to 20% and 41% respectively.

In case of the $^{13}\text{C}(p,\gamma)^{14}\text{N}$ reaction, which presents transitions to different excited states of ^{14}N , considerable efforts have been done to measure the ground state one, with a reported intensity of $\sim 77\%$ [12]. The primary datasets from [7, 12] show good amount of agreement above 250 keV. Nevertheless, the most recent study [13] presents a systematic deviation of 10%. At lower energies, the data start to differ up to 20%. In addition, at the lowest energies the data struggle to agree with the older datasets [14, 15], as can be seen in Fig. 1. The older studies, indeed, deviate by $\sim 30\%$ from the most recent ones. For what regards the minor transitions, only one measurement is available [12]. However, the results are affected by large scattering and the statistical uncertainty ranges from 15% to 40%.

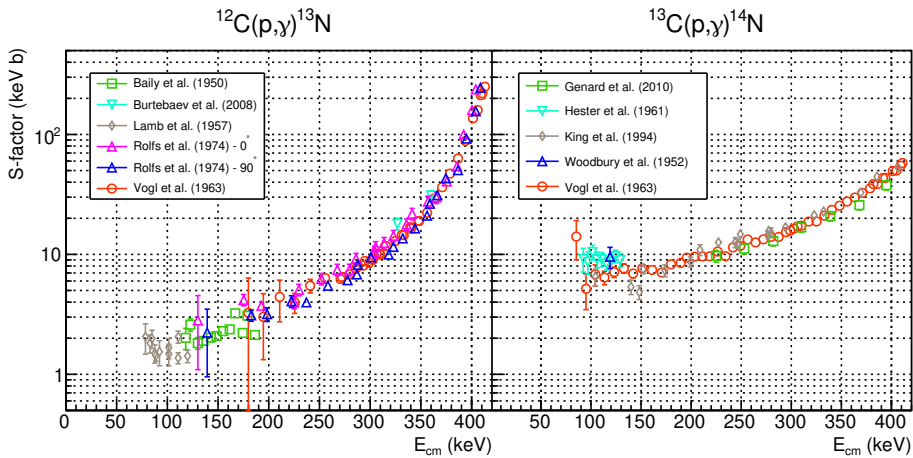


Figure 1: The state of the art for the $^{12}\text{C}(p,\gamma)^{13}\text{N}$ (on the left) and the $^{13}\text{C}(p,\gamma)^{14}\text{N}$ (on the right). For the latter, only the transition to the ground state is shown.

3 Experimental Setup

The main objective of the experimental campaign at LUNA was to measure both the $^{12}\text{C}(p,\gamma)^{13}\text{N}$ and the $^{13}\text{C}(p,\gamma)^{14}\text{N}$ at astrophysical energies with complementary techniques. By doing this, measurements can be cross-checked and systematic uncertainties reduced. In addition, the deep underground location and high current of LUNA 400 kV accelerator [16] guarantees an environmental background level orders of magnitude lower than above ground [17] enabling high-sensitivity measurements. During the experiment both thin evaporated targets and thick targets were employed to check target stability and normalization.

The first set of measurements was conducted using a HPGe detector (in Fig. 2a) positioned in close geometry (~ 1.35 cm). The advantage of this approach lies in the possibility of performing a complete spectroscopic study for both reactions. Especially in case of the

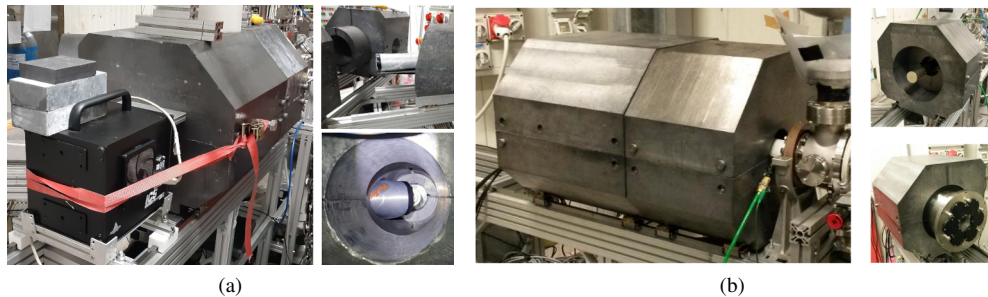


Figure 2: Pictures of (a) the HPGe setup and (b) the BGO setup used during the measurements. Both of the setups employed a Pb shielding for the background reduction.

$^{13}\text{C}(p, \gamma)^{14}\text{N}$, it permits to obtain precise proton capture branchings to each ^{14}N excited state. In addition, the high resolution of the HPGe allowed to study the target degradation with the γ -shape analysis [18]. Finally, the setup allowed to measure both at 0° and 55° and check the the angular distribution of the γ -rays.

The second set of measurements was performed with a large BGO detector [19] (in Fig. 2b). Its close-to- 4π geometry and segmentation in 6 crystals are particularly advantageous for measuring very low cross-sections. In case of the $^{13}\text{C}(p, \gamma)^{14}\text{N}$, the detection in coincidence of all of the energy released as γ -rays allowed to place the region of interest in an almost background-free region [20], owing to the high Q -value of the reaction (~ 7.5 MeV). For the $^{12}\text{C}(p, \gamma)^{13}\text{N}$, given the smaller Q -value (~ 1.9 MeV), different approach had to be used. Since the ^{13}N is β^+ unstable with a half-life of about 10 minutes, the procedure consisted in detecting the two 511 keV γ -rays in coincidence in opposite crystals of the detector. This distinct experimental signature of the positron-electron annihilation grants a significant reduction of the background event rate.

4 Analysis Methods

Given the peculiarity of each measurement, three analysis procedures have been developed:

- For the HPGe data, the γ -shape analysis was performed. The approach consists in a detailed study of the primary γ -peak lines emitted in the two reactions. It allowed both to check the thickness and stoichiometry of the targets. Furthermore, the innovative application of this technique permitted to extract the astrophysical S -factor directly from the minimization, without the need of integrating the γ -peak. An example of the fit can be seen in Fig. 3.
- In case of the ^{13}N activation, an alternative technique was used as the analysis procedure relied on an iterative fitting procedure: at each step, the differential equation that governs the ^{13}N abundance is solved and the activity calculated. The yield of the reaction is treated as a free parameter and thus the best-fit value can be obtained from likelihood maximization. An example of the fit can be seen in Fig. 3.
- Concerning the total absorption spectroscopy with the BGO detector, the sum γ -peak was parametrized and fitted. In this way, the total counts could be readily extracted from the spectra. This strategy requires to establish the sum-peak efficiency of the detector, which relies on Monte Carlo simulations and calibration measurements, and utilizes the branching information from the HPGe measurement as inputs.

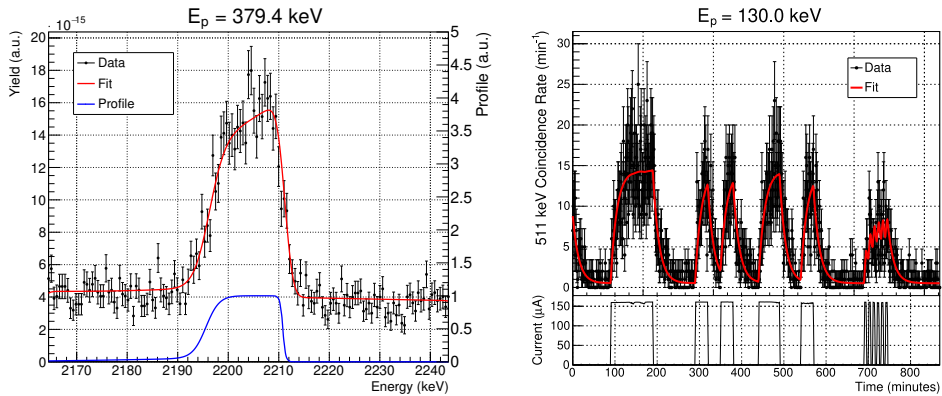


Figure 3: On the left an example of the γ -shape analysis for the HPGe data of the primary transition to the 5691 keV state of ^{14}N . The shape of the γ -peak is modeled both by the exponential drop in the cross-section and by the target profile (in blue). On the right an example of the fit for the $^{12}\text{C}(p, \gamma)^{13}\text{N}$ activation measurement with the BGO. During the irradiation, the event rate increases and then saturates. Whereas when the beam is stopped, the exponential decay is observed.

Finally, the analysis is currently in its final stages and will be presented in a forthcoming publication. The preliminary results show a good agreement among all the different experimental approaches.

References

- [1] K. Lodders, H. Palme, H.P. Gail, *Landolt-Börnstein* **4B**, 712 (2009)
- [2] J.M. Trigo-Rodríguez et al., *Meteorit. Planet. Sci.* **44**, 627 (2009)
- [3] F. Herwig, *Annu. Rev. Astron. Astrophys.* **43**, 435 (2005)
- [4] N. Langer et al., *Astron. Astrophys.* **346**, L37 (1999)
- [5] D. Vescovi et al., *Astrophys. J. Lett.* **897** (2020)
- [6] P.A. Denissenkov, C.A. Tout, *Mon. Not. R. Astron. Soc.* **340**, 722 (2003)
- [7] J.L. Vogl, Ph.D. thesis, California Institute of Technology (1963)
- [8] C. Rolfs, R. Azuma, *Nucl. Phys. A* **227**, 291 (1974)
- [9] N. Burtebaev et al., *Phys. Rev. C* **78**, 035802 (2008)
- [10] C.L. Bailey, W.R. Stratton, *Phys. Rev.* **77**, 194 (1950)
- [11] W.A.S. Lamb, R.E. Hester, *Phys. Rev.* **107**, 550 (1957)
- [12] J.D. King et al., *Nucl. Phys. A* **567**, 354 (1994)
- [13] G. Genard et al., *J. Phys. Conf. Ser.* **202**, 012015 (2010)
- [14] E.J. Woodbury, W.A. Fowler, *Phys. Rev.* **85**, 51 (1952)
- [15] R.E. Hester, W.A. Lamb, *Nucl. Phys. A* **121**, 584 (1961)
- [16] A. Formicola et al., *Nucl. Instrum. Methods Phys. Res. A* **507**, 609 (2003)
- [17] C. Brogini et al., *Prog. Part. Nucl. Phys.* **98**, 55–84 (2018)
- [18] G.F. Ciani, L. Csedreki et al., *Eur. Phys. J. A* **56** (2020)
- [19] C. Casella et al., *Nucl. Instrum. Methods Phys. Res. A* **489**, 160 (2002)
- [20] A. Boeltzig et al., *J. Phys. G* **45**, 025203 (2018)